Available online at www.sciencedirect.com
ScienceDirect
Trans. Nonferrous Met. Soc. China 31(2021) 306−316
Transactions of Nonferrous Metals Society of China
www.tnmsc.cn

Interface kinetics modeling of binary alloy solidification by considering correlation between thermodynamics and kinetics

Shu LI[1,2], Yu-bing ZHANG[1], Kang WANG[1], Feng LIU[1]

1. State Key Laboratory of Solidification Processing, Northwestern Polytechnical University, Xi'an 710072, China;
2. School of Science, Harbin University of Science and Technology, Harbin 150080, China

Received 27 March 2020; accepted 6 August 2020

Abstract: By considering collision-limited growth mode and short-range diffusion-limited growth mode simultaneously, an extended kinetic model for solid−liquid interface with varied kinetic prefactor was developed for binary alloys. Four potential correlations arising from effective kinetics coupling the two growth modes were proposed and studied by application to planar interface migration and dendritic solidification, where the linear correlation between the effective thermodynamic driving force and the effective kinetic energy barrier seems physically realistic. A better agreement between the results of free dendritic growth model and the available experiment data for Ni−0.7at.%B alloy was obtained based on correlation between the thermodynamics and kinetics. As compared to previous models assuming constant kinetic prefactor, a common phenomenon occurring at relatively low undercoolings, i.e. the interface migration slowdown, can be ascribed to both the thermodynamic and the kinetic factors. By considering universality of the correlation between the thermodynamics and kinetics, it is concluded that the correlation should be considered to model the interface kinetics in alloy solidification.

Key words: modelling; interface; dendritic solidification; binary alloy; thermodynamics; kinetics; correlation

1 Introduction

Interface kinetics, along with thermal and solutal transport and morphological stability, determines the final behavior of solidification for alloy melts [1]. The classical Fick diffusion equation or the extended hyperbolic diffusion equation was used to describe the thermal and solutal transport in liquid ahead of the solid−liquid (S/L) interface, due to latent heat releasing and solute redistribution at the interface. Taking into account the nonisothermal and nonisosolutal S/L interface boundary conditions, more accurate solutions of the steady state Fick diffusion equation for the solidification front of a paraboloid of revolution were further obtained [2−7]. The marginal stability theory [8−10], the microscopic solvability theory [11−14], and the phase field theory [15,16] have also been developed to describe the morphological stability of S/L interface very well.

Turnbull's collision-limited growth model [17] is commonly used to describe the interface kinetics for both metals and alloys, to treat the relation between interface migration velocity and thermodynamic driving force, as follows:

$$V=V_0[1-\exp(\Delta G/(RT_i))] \quad (1)$$

where V is the interface migration velocity, the kinetic prefactor V_0 is assumed to be a constant with a value of sound speed in melts, ΔG is the change of Gibbs free energy of alloy, R is the mole gas constant and T_i is the interfacial temperature. The collision-limited growth regime assumes that the crystallization rate is controlled by the impingement

Corresponding author: Feng LIU; Tel: +86-29-88460374; E-mail: liufeng@nwpu.edu.cn
DOI: 10.1016/S1003-6326(21)65497-3
1003-6326/© 2021 The Nonferrous Metals Society of China. Published by Elsevier B.V. & Science Press

frequency of atoms with the crystal surface. This regime is not thermally activated, and V_0 can be regarded as the maximum solidification velocity at infinite thermodynamic driving force. Strictly speaking, Turnbull's collision-limited growth model is only suitable for single-component melts or pure metals, since for alloy melts there should be another regime controlling the solidification behavior under low undercooling conditions, i.e. the short-range diffusion-limited growth regime. That is to say, Eq. (1) is only suitable for solidification under sufficiently high undercooling conditions, where complete solute trapping occurs and solute redistribution disappears at the S/L interface. Under low undercooling conditions, however, the solute partitioning is required for alloy solidification, which can only be accomplished by the inter-diffusion between solute and solvent atoms at the interface. This is a thermally activated process, which can lead to a phenomenon of the interface slowdown. As proposed by AZIZ and BOETTINGER [18], it is more reasonable to describe the interface kinetics for alloy solidification under low undercooling conditions as follows:

$$V=V_{\mathrm{DI}}[1-\exp(\Delta G/(RT_{\mathrm{i}}))] \tag{2}$$

where V_{DI} is the diffusive speed at the interface. Correspondingly, the solidification mechanism follows the short-range diffusion-limited growth model.

The above two growth modes belong to extreme conditions, whereas the solidification itself is always simultaneously controlled by thermal and solutal transport. This gives rise to an open question, i.e. how to unify the above two solidification regimes, i.e. Eqs. (1) and (2), into one equation to describe the interface kinetics. Previous models in Refs. [19−25] treated this problem by holding Eq. (1) but replacing ΔG with an effective one ΔG_{eff} (or still using ΔG). Accordingly, the models with ΔG_{eff} describe the interface slowdown by a so-called solute drag effect, which assumes that the total ΔG is dissipated partially by the solute−solvent redistribution. Whether the solute drag effect needs to be considered remains an argument [26−32]. One thing is certain, that all of these previous models [19−25] attribute the interface mobility varying with increasing undercoolings to one aspect, i.e. the thermodynamic effect. However, not only ΔG, but also the kinetic prefactor V_0 and V_{DI} (Eqs. (1) and (2)) determine the as-solidified microstructure. Then, one question must be highlighted, i.e. how to reflect the effect of the effective kinetics on solidification?

The present work aimed to model the interface kinetics by incorporating the two extreme modes into one kinetic equation; the varied kinetic prefactor thus reflects the transition of mobility and energy barrier between the two extreme modes. Following the current theoretical framework, the correlations between the kinetic prefactor and the thermodynamic driving force were proposed and studied by application to planar interface migration and dendritic solidification for binary alloys. A linear correlation between the effective thermodynamic driving force and the effective energy barrier seems physically realistic, by comparison with the available experiment data of Ni−B alloys. On this basis, universality of the correlation was discussed. It is finally concluded that the correlation should be taken into account to model the interface kinetics in alloy solidification.

2 Model derivation

2.1 Interface kinetics

2.1.1 Effective energy barrier and effective thermodynamic driving force

For alloy melts under sufficiently high undercooling conditions, V is so fast that the solute partitioning is suppressed and the complete solute trapping occurs. Then, the interface kinetics upon solidification is similar to that for pure metals, which can be described by Eq. (1). Under this condition, the solidification process is mainly controlled by the thermal transport and the mechanism can be regarded as thermal-controlled, so Eq. (1), with an effective energy barrier $Q_{\mathrm{eff}}=Q_{\mathrm{T}}$, can be rewritten as follows:

$$V=V_0\exp(-Q_{\mathrm{T}}/(RT_{\mathrm{i}}))[1-\exp(\Delta G/(RT_{\mathrm{i}}))] \tag{3}$$

where Q_{T} is the activation energy for thermal diffusion, which can be approximately considered as negligible.

For alloy melts under sufficiently low undercooling conditions, the solidification behavior is mainly determined by the interdiffusion between solute and solvent atoms. The short-range diffusion-limited growth regime can be regarded as

solute-controlled, which, as a thermally activated process, reduces the interface mobility and also the kinetic prefactor. Thus, the kinetic prefactor V_{DI}, i.e. the solutal diffusion velocity at the interface, can be defined by [30]

$$V_{DI}=V_0\exp(-Q_D/(RT_i)) \tag{4}$$

It then follows that Eq. (2) with an effective energy barrier $Q_{eff}=Q_D$, can be rewritten as follows:

$$V=V_0\exp(-Q_D/(RT_i))[1-\exp(\Delta G/(RT_i))] \tag{5}$$

where Q_D is the activation energy for solutal diffusion, which, in contrast with $Q_T(=0)$, cannot be ignored here. The value of V_0 is normally three orders of magnitude greater than that of V_{DI}.

At intermediate undercoolings, there must be a transition between the solute-controlled and the thermal-controlled modes. This implies that the interface kinetics should not be solely determined by Eq. (3) or Eq. (5), but be correlated with both. In order to describe the interface kinetics using one equation suitable for the entire undercooling conditions, an effective energy barrier Q_{eff} is thus introduced, which is defined by

$$Q_{eff}(\eta)=\eta Q_D+(1-\eta)Q_T \tag{6}$$

where the key parameter $\eta(0,1)$ represents a typically kinetic state of solidification, reflecting different contributions from thermal- and solutal-controlled mechanisms. Then, a unified equation for the interface kinetics is given by

$$V=V_0\exp(-Q_{eff}/(RT_i))[1-\exp(\Delta G/(RT_i))] \tag{7}$$

Define an effective kinetic prefactor V_0^{eff} as

$$V_0^{eff}=V_0\exp[-Q_{eff}/(RT_i)] \tag{8}$$

Then Eq. (7) can be rewritten as follows:

$$V=V_0^{eff}(\eta)[1-\exp(\Delta G/(RT_i))] \tag{9}$$

where $V_0^{eff}(\eta)$ can be written as

$$V_0^{eff}=V_0(V_{DI}/V_0)^{\eta} \tag{10}$$

or

$$V_0^{eff}=V_0[\exp(-Q_D/(RT_i))]^{\eta} \tag{11}$$

At sufficiently high undercoolings, the parameter η equals zero and V_0^{eff} equals V_0, so Eq. (7) reduces to Eq. (3) or Eq. (1), representing the collision-limited growth regime. Then, a continuously increased η with decreasing undercooling indicates a transition of solidification mechanism from the thermal-controlled growth to the solute-controlled growth. At sufficiently low undercoolings, η tends to be 1 and V_0^{eff} reduces to V_{DI}, so Eq. (7) reduces to Eq. (5) or Eq. (2), representing the short-range diffusion-limited growth regime. Note that, in order to study the effect of solute drag ΔG in Eq. (9) is also replaced by ΔG_{eff}, as done in previous models [23−27]:

$$\Delta G_{eff}=\Delta G-\beta\Delta G_D \tag{12}$$

where ΔG_D is the solute drag free energy and β is the solute drag factor.

2.1.2 Correlations between thermodynamics and kinetics

Suppose that the complete solute trapping corresponds to the critical state marked by ΔG_{eff}^*, i.e. the solute partition coefficient $k=1$, $\eta=0$ and $V=V_D$, in contrast with the state of negligible ΔG_{eff}, i.e. $k=k_e$, $\eta\to1$ and $V\to0$. With increasing ΔG_{eff} from zero to ΔG_{eff}^*, the solidification mechanism is changed from the solute-controlled growth to the thermal-controlled growth and the parameter η varies continuously from 1 to 0. In order to derive the correlation between Q_{eff} and ΔG_{eff}, a functional relation between η and ΔG_{eff} must be specified according to Eq. (6), and Mode 1 is proposed by assuming a linear relationship between η and ΔG_{eff} in the range of $[0, \Delta G_{eff}^*]$, i.e. at $V<V_D$,

$$\eta_{Mode\,1}=1-\Delta G_{eff}/\Delta G_{eff}^* \tag{13}$$

where ΔG_{eff}^* corresponds to the critical undercooling ΔT^* with $V=V_D$; for $V\geq V_D$, η holds constant as zero, indicating the collision-limited growth regime. Based on Mode 1, a linear correlation between Q_{eff} and ΔG_{eff} can be given as $Q_{eff}=Q_D-\Delta G_{eff}/\Delta G_{eff}^*(Q_D-Q_T)$. Similarly, Mode 2 assumes an exponential relation of η with ΔG_{eff}, at $\Delta G_{eff}<\Delta G_{eff}^*$,

$$\eta_{Mode\,2}=\frac{\exp[\Delta G_{eff}/(RT_i)]-\exp[\Delta G_{eff}^*/(RT_i)]}{1-\exp[\Delta G_{eff}^*/(RT_i)]} \tag{14}$$

where, for $\Delta G_{eff}\geq\Delta G_{eff}^*$, $\eta\equiv0$ always holds; under the condition that V/V_0^{eff} tends to zero, ΔG_{eff} tends to zero and Mode 2 reduces to Mode 1.

Considering possible relations between η and other thermodynamic parameters, another two potential modes are still available. Assuming a linear relation between η and k, i.e. for $k=k_e$, $\eta=1$; for $k=1$, $\eta=0$ and for $k_e<k<1$, the following relation holds

$$\eta_{\text{Mode 3}}=\frac{1-k}{1-k_e} \tag{15}$$

With the assumption of a linear relation between η and the difference $C_L^*-C_S^*$, at V=0, $C_L^*-C_S^*=C_L^{eq}-C_S^{eq}$ and η=1; at $V=V_D$, $C_L^*-C_S^*=0$ and η=0; and η can be described as follows, under the condition that $C_L^*-C_S^*$ takes other values,

$$\eta_{\text{Mode 4}}=\frac{C_L^*-C_S^*}{C_L^{eq}-C_S^{eq}}=\frac{C_L^*(1-k)}{C_L^{eq}(1-k_e)} \tag{16}$$

where C_L^*, C_S^*, C_L^{eq} and C_S^{eq} stand for the solute concentrations at the S/L interface; and the superscript "eq" represents the equilibrium values.

Incorporating Eqs. (13)−(16) into Eqs. (6) and (9), different correlations between thermodynamics and kinetics can be obtained.

2.2 Solidification with planar interface

In steady state solidification with planar interface for binary alloy melts, C_S^* is a constant and equals the equilibrium value C_S^{eq} as well as nominal composition of alloys C_0 [17]. Under this condition, Mode 4 defined by Eq. (16) reduces to the following expression:

$$\eta_{\text{Mode 4}}=\frac{k_e(1-k)}{k(1-k_e)} \tag{17}$$

For non-dilute alloys, ΔG_{eff} can be calculated numerically and thermodynamically by using subregular solution model based on CALPHAD method [23,33]. For dilute alloys, Henry's law and Baker and Cahn's approximation for the chemical potentials of solute and solvent lead to an analytical expression as follows [24]:

$$\Delta G_{\text{eff}}=RT_i\{C_S^{eq}-C_L^{eq}+C_L^*[1-k+(k+(1-k)\beta)\cdot \ln(\frac{k}{k_e})+(1-k)^2\frac{V}{V_D}]\} \tag{18}$$

where β is the solute drag factor, which is introduced to unify the two treatments with (β=1) and without (β=0) solute drag. For linear liquidus and solidus within the composition range of interest, Eq. (18) can be rewritten as

$$\Delta G_{\text{eff}}=RT_i(1-k_e)(T_M+C_L^*m_L(V)-T_i)/m_L^e \tag{19}$$

where T_M is the melting temperature of solvent, m_L^e is the slope of equilibrium liquidus and $m_L(V)$ is regarded as kinetic liquidus slope defined by

$$m_L(V)=\frac{m_L^e}{1-k_e}[1-k+(k+(1-k)\beta)\ln(\frac{k}{k_e})+(1-k)^2\frac{V}{V_D}] \tag{20}$$

Equations (18) and (20) can be further simplified at $V\geq V_D$, due to the complete solute trapping with k=1.

For small velocities relative to $V_0^{\text{eff}}(\eta)$, Eq. (9) is further approximated by

$$V=-V_0^{\text{eff}}(\eta)\Delta G_{\text{eff}}/(RT_i) \tag{21}$$

Substituting Eq. (19) into Eq. (21), the interface temperature T_i can be described as

$$T_i=T_M+C_L^*m_L(V)+\frac{m_L^e}{1-k_e}\frac{V}{V_0^{\text{eff}}(\eta)} \tag{22}$$

For dilute binary alloys, considering the relaxation effect of local nonequilibrium solute diffusion in bulk liquid, the solute partition coefficient k is given by SOBOLEV as [34]

$$k=\frac{(1-V^2/V_D^2)k_e+V/V_{DI}}{1-V^2/V_D^2+V/V_{DI}},\ V<V_D \tag{23a}$$

$$k=1,\ V\geq V_D \tag{23b}$$

Combining Eqs. (20), (22), (23a) and (23b) with Modes 1−4, one can describe the final behavior of solidification with planar interface.

2.3 Free dendritic growth model

For further modeling the free dendritic growth, another physical quantity i.e. curvature radius r should be introduced to denote the tip morphology of dendrite (curvature radius). Based on the marginal stability theory, the curvature radius r is described as [9]

$$r=\frac{\Gamma/\sigma^*}{\frac{\Delta H_f}{c_p}P_t\xi_t+\frac{2m_L(V)C_L^*(k-1)}{1-V^2/V_D^2}P_c\xi_c},\ V<V_D \tag{24a}$$

$$r=\frac{\Gamma/\sigma^*}{P_t\xi_t(\Delta H_f/c_p)},\ V\geq V_D \tag{24b}$$

where Γ is the Gibbs−Thompson coefficient; σ^* is the stability constant ($\sigma^*\approx 1/(4\pi^2)$); P_t[$=rV/(2\alpha)$] is the thermal Péclet number; P_c[$=rV/(2D)$] is the solute Péclet number; α and D are respectively the thermal diffusivity and solute diffusion coefficient in the liquid; ΔH_f is the latent heat of fusion; c_p is the heat capacity of liquid alloy; and the parameters ξ_t and ξ_c are defined by

$$\xi_t=1-\frac{1}{\sqrt{1+1/(\sigma^* P_t^2)}} \tag{25}$$

$$\xi_c=1-\frac{2k}{2k-1+\sqrt{1+(1-V^2/V_D^2)/(\sigma^* P_c^2)}},\ V<V_D \tag{26a}$$

$$\xi_c=0,\ V\geq V_D \tag{26b}$$

From the current interface kinetics, Eqs. (21), (24a) and (24b), the interface response function assuming linear liquidus and solidus can be modified as

$$T_i=T_M+C_L^* m_L(V)+\left(\frac{m_L^e}{1-k_e}\right)\frac{V}{V_0^{eff}(\eta)}-\frac{2\Gamma}{r} \tag{27}$$

From this equation, the total bath undercooling ΔT is described as

$$\Delta T=[m_L^e C_0-m_L(V)C_L^*]+\frac{2\Gamma}{r}-\left(\frac{m_L^e}{1-k_e}\right)\frac{V}{V_0^{eff}(\eta)}+\frac{\Delta H_f}{c_p}\mathrm{Iv}(P_t) \tag{28}$$

where Iv is the Ivantsov function. In the right-hand side of Eq. (28), the four terms represent the constitutional undercooling, the curvature undercooling, the kinetic undercooling and the thermal undercooling (i.e. obtained from the solution of thermal transport equation in the liquid region), in order. ΔT is defined by $\Delta T=T_M+m_L^e C_0-T_\infty$, where T_∞ is the temperature in liquid far from the interface. Another result by solving the solute diffusion equation in the liquid region gives the description of liquid solute concentration at the interface (C_L^*) [21]:

$$C_L^*=\frac{C_0}{1-(1-k)\mathrm{Iv}(P_c)} \tag{29}$$

Assuming linear liquidus and solidus, the solute trapping model is also described by Eqs. (23a) and (23b).

Up to now, the extended kinetic model considering the correlation between thermodynamics and kinetics (i.e. the effective kinetic prefactor $V_0^{eff}(\eta)$) has been determined. If the correlations between thermodynamics and kinetics were ignored, i.e. $V_0^{eff}(\eta)\equiv V_0$ holds with all values of η in Eqs. (22), (27) and (28), the present model would reduce to previous ones [21], in which only the collision-limited growth mechanism is considered. Note that the present model established above is only suitable for dilute binary alloys with linear liquidus and solidus lines for simplicity. For non-dilute alloys with non-linear liquidus or multi-component alloys, the interfacial kinetic equation described by the correlation between thermodynamics and kinetics, Eq. (9), is also reasonable. In that case, however, the extended solute trapping model [30] and marginal stability theory [33] should be adopted.

3 Model description and application

3.1 Planar interface migration

For the planar interface migration upon solidification of Al−0.5at.%Be alloy (Table 1 [18]), model comparisons have been performed to distinguish the present model from the corresponding model [24] based on Turnbull's collision-limited growth mode. Since the present model considers both growth modes, a varied kinetic prefactor $V_0^{eff}(\eta)$ is then according to Eq. (10) or Eq. (11) prevailing, in contrast with a constant kinetic prefactor V_0 used in previous models [24]. Actually, the main improvement for the present model relative to previous ones lies in $V_0^{eff}(\eta)$; if the varied $V_0^{eff}(\eta)$ is replaced by a constant V_0 at all values of η, the present model reduces to previous ones [21]. Therefore, the ratio V_0^{eff}/V_0 is an important factor for the present model to be distinguished from previous ones.

Table 1 Parameter data for Al−0.5at.%Be alloy used in model computations [18]

Parameter	Value
Melting point of pure Al, T_M/K	933.58
Liquidus slope, m_L^e/(K·at.%$^{-1}$)	−6.44
Partition coefficient, k_e	0.0429
Diffusion speed in bulk liquid, V_D/(m·s^{-1})	∞
Kinetic prefactor, V_0/(m·s^{-1})	1000

So, effect of model parameters on this ratio V_0^{eff}/V_0 is discussed first, and then effect of different mechanisms on the interfacial temperature, and finally, four potential correlations arising from Modes 1−4, are discussed. All of these results shown in Figs. 1−3 are calculated by the correlation arising from Mode 4 for simplicity. It should be noted that, analogous conclusions can also be obtained using the correlations arising from

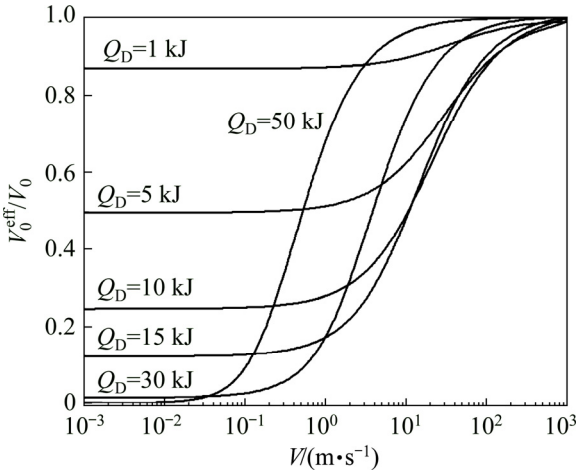

Fig. 1 Evolution of effective kinetic prefactor V_0^{eff} as functions of interface velocity V for six different values of solutal diffusion activated energy Q_D for Al−0.5at.%Be alloy (The results are calculated by Eqs. (10), (17), (20), (22) and (23))

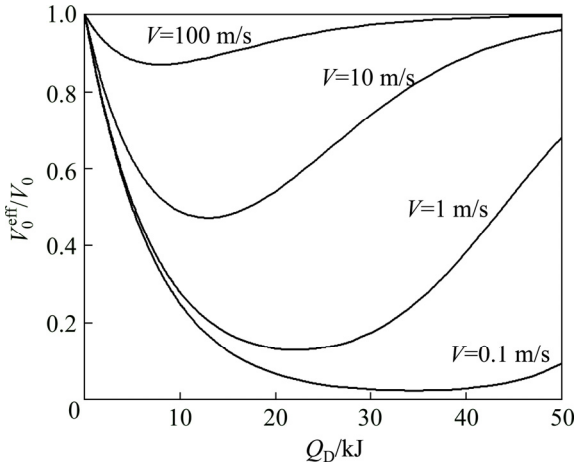

Fig. 2 V_0^{eff}/V_0 as function of Q_D for Al−0.5at.%Be alloy at different interface velocities

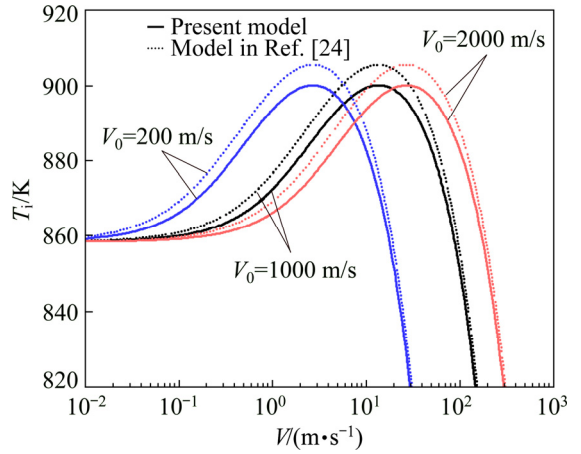

Fig. 3 T_i as function of V for Al−0.5at.%Be alloy at Q_D=20 kJ and different V_0 values

Modes 1−3, still. In addition, all of these results shown in Figs. 1−4 are calculated without solute drag effect (β=0).

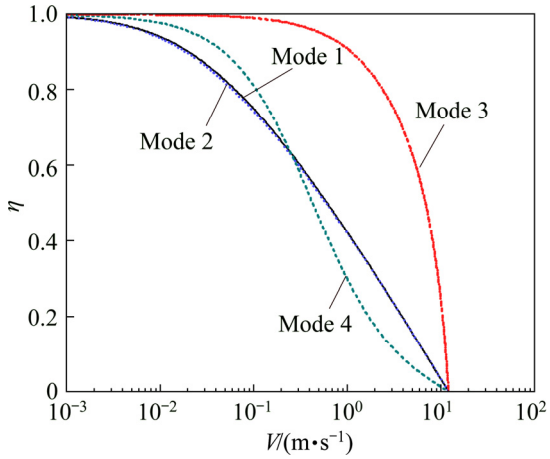

Fig. 4 η as function of interface velocity with Modes 1−4 for Al−0.5at.%Be alloy (V_{DI}=10 m/s; V_D=12 m/s)

3.1.1 Ratio V_0^{eff}/V_0

As for the effect of Q_D (the activation energy for inter-diffusion), the ratio V_0^{eff}/V_0 as function of interface velocity V for different values of Q_D are shown in Fig. 1. It is indicated that the ratio V_0^{eff}/V_0 decreases with increase of Q_D at sufficiently low V, e.g. V=0.01 m/s, where the kinetic parameter η approximately equals 1 and thus the parameter Q_D is the main determining factor according to Eq. (11). However, the above monotonicity disappears at relatively high velocities. In order to show this interesting phenomenon more clearly, the ratios V_0^{eff}/V_0 as function of Q_D at four selected interface velocities are shown in Fig. 2, where V_0^{eff}/V_0 decreases firstly and then increases with increasing Q_D, since the increased Q_D not only decreases V_0^{eff} directly through $V_0^{eff}=V_0[\exp(-Q_D/(RT_i))]^{\eta}$, but also increases V_0^{eff} indirectly by decreasing η through suppressing the solute partitioning. Therefore, there are two opposite factors determining V_0^{eff} as well as the ratio V_0^{eff}/V_0. Further analysis can be found in Appendix in detail.

Further from Fig. 1, if Q_D is equal to zero, V_0^{eff} will be invariable at all velocities ($V_0^{eff}/V_0 \equiv 1$); the short-range diffusion-limited growth regime will disappear; there will be only the collision-limited growth regime [24].

3.1.2 Interfacial temperature T_i

The interfacial temperature T_i as function of V is shown in Fig. 3, for different values of V_0 and a

fixed Q_D (Q_D=20 kJ). The predicted T_i by the present model is lower than that by the one assuming an invariable kinetic prefactor V_0, due to the lower V_0^{eff} for the present model in contrast with the maximum V_0 used in the corresponding model [24] (the ratio V_0^{eff}/V_0 is less than 1). That is to say, given the lower kinetic prefactor (equivalent to the interfacial mobility), T_i must be lower, to guarantee higher ΔG_{eff} to achieve the same V. It is also indicated in Fig. 3 that, the difference between T_i predicted by the two models is independent of the parameter V_0, and if the horizontal coordinate V is replaced by the normalized V/V_0, the three curves with different values of V_0 will coincide with each other. This implies that the influence of T_i in Eq. (10) is negligible and one can use the parameter V_{DI} defined by Eq. (4) instead of the parameter Q_D, i.e. use Eq. (10) to replace Eq. (11).

3.1.3 Selection of key parameter η

Under a specific solidification condition, the parameter Q_D is normally fixed and the key parameter η is varied with the thermodynamic state. The parameter η as function of V is shown in Fig. 4, to discuss these correlations arising from Modes 1−4 more clearly. One can see that the same basic law holds that the value of η decreases continuously from 1 to 0 with increasing V. As V tends to zero, the kinetic parameter $\eta\rightarrow 1$ ($V_0^{eff}=V_{DI}$), indicating the short-range diffusion-limited growth; the collision-limited growth occurs with η=0 ($V_0^{eff}=V_0$), at $V\geq V_D$. For intermediate values of η, there is a transition between the two growth regimes. For different modes, the slower the decrease of η with increasing V is, the smaller the ratio V_0^{eff}/V_0 is and thus the more obvious the distinction between the present model and the previous one is [24] (see also Fig. 4 and Figs. A1 and A2). Clearly, the effect of Mode 3 is relatively more remarkable compared with other three modes. The curves of Modes 1 and 2 almost coincide with each other, due to the approximation of $\exp(\Delta G_{eff}/(RT_i))\approx\Delta G_{eff}/(RT_i)+1$ given the finite value of V_D in bulk liquid. It is thus concluded that Mode 1 for η is more essential, implying a linear correlation between Q_{eff} and ΔG_{eff}, approximately.

No matter which mode prevails, for the present kinetics, both Q_D (or V_{DI}) and η determine Q_{eff} by Eq. (6), which further controls V_0^{eff}, Eq. (8), so that the ratio V_0^{eff}/V_0 finally determines the difference between the present model and the model assuming constant V_0 [24].

3.2 Experimental application

3.2.1 Model assumption for free dendrite growth

Employing the physical data for solidification of Ni−0.7at.%B alloy (Table 2), model calculations (not shown here) indicate that, similar to the result shown in Fig. 4, the difference between the present model predictions with Modes 1 and 2 is also very small, due to the approximation $\exp(\Delta G_{eff}/(RT_i))\approx\Delta G_{eff}/(RT_i)+1$; the effect of Mode 3 is too remarkable for the present model to give a reasonable prediction, and Mode 4, Eq. (16), is not suitable for dendritic growth due to the non-monotonicity of the difference $C_L^*-C_S^*$ with increasing bath undercooling ΔT under dendritic growth conditions. If the version of Mode 4 with planar solid/liquid interface, Eq. (16), is adopted approximately, the difference between the predictions from the present model and Galenko−Danilov model (GD model [21]) will be very small. Therefore, Mode 1 (or Mode 2) implying the correlation between Q_{eff} and ΔG_{eff}, seems physically realistic, which is thus inputted into the present model, as compared with GD model assuming constant V_0, to predict the dendritic growth velocity V as function of ΔT (Fig. 5), upon solidification of Ni−0.7at.%B alloy [35]. Equations (20), (23)−(29) are adopted in the model calculation assuming linear liquidus and solidus, due to the sufficiently dilute nominal composition of Ni−0.7at.%B alloy.

Table 2 Thermophysical data for Ni−0.7at.%B alloy used in model computations [21]

Parameter	Value
Melting point of pure Ni, T_M/K	1726
Heat of fusion, ΔH_f/(J·mol^{-1})	1.72×10^4
Heat capacity, c_p/(J·mol^{-1}·K^{-1})	36.39
Capillarity constant, Γ/(K·m)	3.42×10^{-7}
Liquidus slope, m_L^e/(K·at.%$^{-1}$)	−14.3
Partition coefficient, k_e	0.0155
Diffusion coefficient, D/(m^2·s^{-1})	3.0×10^{-9}
Thermal diffusivity, α/(m^2·s^{-1})	8.5×10^{-6}
Interfacial diffusion speed, V_{DI}/(m·s^{-1})	18.9
Diffusion speed in bulk liquid, V_D/(m·s^{-1})	18.9
Kinetic prefactor, V_0/(m·s^{-1})	363.1

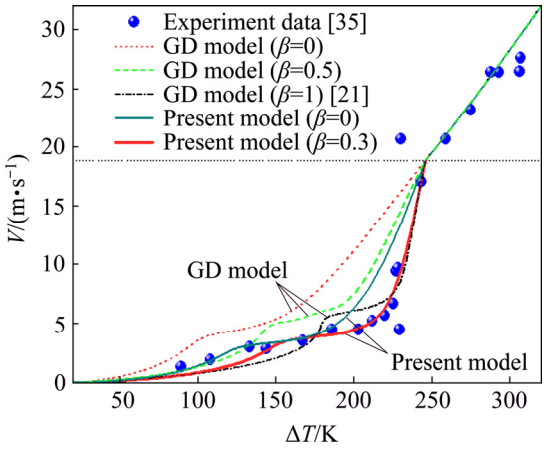

Fig. 5 Calculated and experimental dendritic growth velocities V as functions of bath undercooling ΔT for Ni−0.7at.%B alloy (Mode 1 is adopted to describe the kinetic parameter η)

Upon introducing Q_{eff} in the present model, the theoretical framework of sharp interface is assumed. Neglecting the interface thickness, the sharp interface model can be regarded as a simplified version of diffusive interface model with an average value C^* of solute concentration in the interfacial region, which is defined by $C^*=\beta C_{\text{L}}^*+(1-\beta)C_{\text{S}}^*$ [24,25,30]. In reality, the interfacial solute concentration varies continuously from solid to liquid [25,32]. Therefore, it is more reasonable for the average C^* to take a value between C_{S}^* and C_{L}^*. This implies that the solute drag factor β equals a value between 0 and 1, indicating the partial solute drag effect. In the current theoretical framework, the effective thermodynamic driving force can be dealt with, in combination with the partial solute drag effect. On this basis, if the partial solute drag effect needs to be considered, then different values of solute drag factor β should be chosen [24−27].

3.2.2 Model application

As shown in Fig. 5, for both the present model assuming the linear correlation between Q_{eff} and ΔG_{eff} and the GD model [21] assuming constant V_0, the larger the value of β is, the more remarkable the interface slowdown is; both the effect due to V_0^{eff} and that due to solute drag lead to the interface slowdown. Since both the present model considering Mode 1 and β=0.3 and the GD model assuming β=1 and constant V_0 show sufficiently good prediction for the experimental data, then it is indeed due to the interface slowdown that guarantees good model predictions. The effect due to variable V_0^{eff} is used to treat the interface slowdown by considering variation of Q_{eff}, whereas the effect due to solute drag is used to describe the interface slowdown phenomenon by assuming that a part of total Gibbs free energy change in solidification is dissipated by interdiffusion between solute and solvent atoms at the interface and is not available to drive interfacial motion. Additionally, in fact during the electro-magnetic levitation experiment with Ni−0.7at.%B alloy the melt convection is inevitable inside the droplet [35]. In further works convective flow should be taken into account for Ni−B droplets, which increases the interface velocity especially in the short-range diffusion-limited growth kinetics [1]. Recently, other applications of the thermo-kinetic correlation in twin-roll casting [36] as well as in designing stable nanocrystalline alloys [37] have been carried out successfully. On this basis, it is further supported to finally conclude that the correlation should be taken into account to model the interface kinetics in alloy solidification. Meanwhile, for alloy solidification numerous simulation results have been reported by phase field method, which has its advantage compared with analytic theory, due to its ability to model complex geometrical morphology of solid/liquid interface. Therefore, a comparative study is also meaningful by combining the analytic theory and the phase field method to describe the interfacial kinetics [16].

4 Conclusions

(1) An extended interface kinetic model was developed for binary alloys, by simultaneously considering both the collision-limited growth and the short-range diffusion-limited growth modes.

(2) Applying to planar interface migration, the interface temperature T_{i} predicted by the present model is lower than that by the previous one, due to the ratio V_0^{eff}/V_0 less than 1, and with the increase of the solutal diffusion activated energy Q_{D} the ratio V_0^{eff}/V_0 does not decrease monotonously but decreases firstly and then increases.

(3) The present model can reduce to the previous one, when the parameter Q_{D} equals zero, i.e. $V_{\text{DI}}\equiv V_0$. Four potential relationships of η with ΔG_{eff} or other thermodynamic quantities were assumed to analyze the correlation. It is concluded

that the linear correlation between the effective kinetic energy barrier Q_{eff} and the effective thermodynamic driving force ΔG_{eff} is more essential.

(4) Experimental comparison indicates that the present free dendritic growth model can give a better agreement with the experimental data for Ni−0.7at.%B alloy. The correlation between thermodynamics and kinetics should be taken into account to model interface kinetics in binary alloy solidification.

Acknowledgments

The authors are grateful for the financial supports from the National Natural Science Foundation of China (51671075 and 51790481), the National Key R&D Program of China, (2017YFB0703001 and 2017YFB0305100), China Postdoctoral Science Foundation (2016M590970), the Fund of the State Key Laboratory of Solidification Processing in NWPU, China (SKLSP201606), the Fundamental Research Foundation for Universities of Heilongjiang Province, China (LGYC2018JC004), and the Heilongjiang Postdoctoral Fund for Scientific Research Initiation, China (LBH-Q16118).

Appendix

Non-monotonicity of V_0^{eff} with Q_{D} at relatively high velocities is described as follows.

Relations between V_0^{eff} and η, and between η and V for six given Q_{D} values are shown in Figs. A1 and A2, respectively. Figure A1 indicates that, if the same value of η is given, the larger Q_{D} gives the lower V_0^{eff}. Considering the effect of η, however, parameter Q_{D} can also influence η and further change the value of V_0^{eff} indirectly. Figure A2 shows that, with increasing Q_{D}, η decreases at any given value of interface velocity V. Under a specific solidification condition, the decrease of η means a transition from short-range diffusion-limited growth to collision-limited growth, i.e. the increase of V_0^{eff}.

Therefore, there are two opposite factors, which result in the non-monotonicity shown in Fig. 2. This can also be explained as follows. With increasing Q_{D} from zero, the monotonously decreasing stage of V_0^{eff} is mainly controlled by the parameter Q_{D} in Eq. (11), as a determining factor of Q_{eff} defined by Eq. (6), and the monotonously increasing stage of V_0^{eff} is mainly determined by the parameter Q_{D} used in Eq. (4). With increasing Q_{D}, V_{DI} is decreased according to Eq. (4). This prevents the solute partitioning from Eq. (23a), facilitates the solute trapping at the interface and further results in a higher value of partition coefficient k, implying the collision-limited growth mode. Meanwhile, the parameter η decreases, thus increasing V_0^{eff}. So, the parameter η can also be regarded as another determining factor of Q_{eff} defined by Eq. (6). Most importantly, Q_{eff} determines the final behavior of the effective kinetic prefactor V_0^{eff} by Eq. (8).

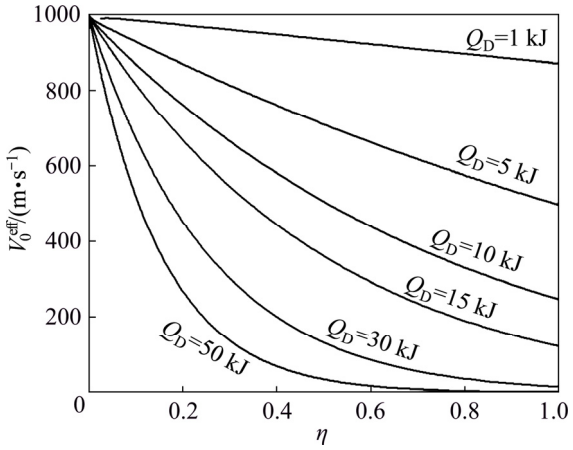

Fig. A1 Effective kinetic prefactor V_0^{eff} as function of kinetic parameter η for six different values of solutal diffusion activated energy Q_{D} for Al−0.5at.%Be alloy

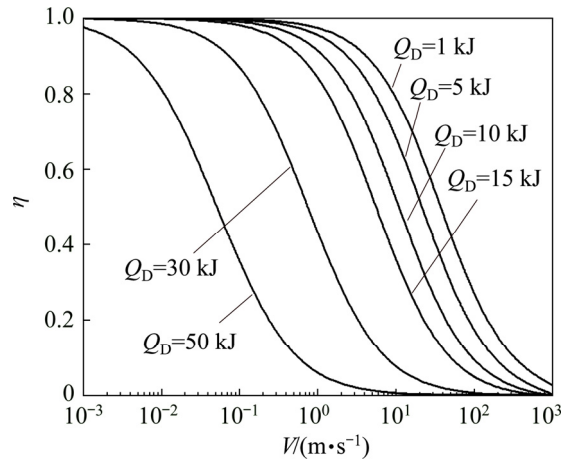

Fig. A2 Kinetic parameters η as function of interface velocity for different Q_{D} for Al−0.5at.%Be alloy (The kinetic parameter η is described by Mode 4)

References

[1] KURZ W, RAPPAZ M, TRIVEDI R. Progress in modelling solidification microstructures in metals and alloys. Part II: dendrites from 2001 to 2018 [J]. International Materials Reviews, 2021, 66: 30−76.

[2] LI Shu, GU Zhi-hui, LI Da-yong, WU Shuang-shuang,

CHEN Ming-hua, FENG Yu. Analysis for free dendritic growth model incorporating the interfacial nonisosolutal nature due to normal velocity variation [J]. Transactions of Nonferrous Metals Society of China, 2015, 25: 3363−3369.

[3] LI Shu, GU Zhi-hui, LI Da-yong, LIU Shu-cheng, CHEN Ming-hua, FENG Yu. Analysis for free dendritic growth model incorporating the nonisothermal nature of solid–liquid interface [J]. Physics Letters A, 2015, 379: 237−240.

[4] LI Shu, LI Da-yong, LIU Shu-cheng, GU Zhi-hui, LIU Wei, HUANG Jian-wei. An extended free dendritic growth model incorporating the nonisothermal and nonisosolutal nature of the solid liquid interface [J]. Acta Materialia, 2015, 83: 310−317.

[5] LIU Shu-cheng, LIU Li-hua, LI Shu, WANG Jin-zhong, LIU Wei. Analysis for free dendritic growth model based on nonisothermal interface and microscopic solvability theory [J]. Transactions of Nonferrous Metals Society of China, 2019, 29: 601−607.

[6] LIU Shu-cheng, LI Shu, LIU Feng. Analysis of free dendritic growth considering both relaxation effect and effect of nonisothermal and nonisosolutal interface [J]. International Journal of Heat and Mass Transfer, 2019, 134: 51−57.

[7] LIU Shu-cheng, LIU Li-hua, LI Shu, WANG Jin-zhong. Free dendritic growth model for binary alloy based on microscopic solvability theory and nonisothermal nature caused by anisotropy and curved interface [J]. Journal of Crystal Growth, 2020, 534: 125417.

[8] MULLINS W W, SEKERKA R F. Stability of a planar interface during solidification of a dilute binary alloy [J]. Journal of Applied Physics, 1964, 35: 444−451.

[9] GALENKO P K, DANILOV D A. Linear morphological stability analysis of the solid-liquid interface in rapid solidification of a binary system [J]. Physical Review E, 2004, 69: 051608.

[10] LI Shu, ZHANG Jiong, WU Ping. Numerical test of generalized marginal stability theory for a planar interface during directional solidification [J]. Scripta Materialia, 2009, 61: 485−488.

[11] LANGER J S, MULLER-KRUMBHAAR H. Theory of dendritic growth—I Elements of a stability analysis [J]. Acta Metallurgica, 1978, 26: 1681−1689.

[12] LANGER J S. Instabilities and pattern formation in crystal growth [J]. Reviews of Modern Physics, 1980, 52: 1−28.

[13] KESSLER D A, KOPLIK J, LEVINE H. Pattern selection in fingered growth phenomena [J]. Advances in Physics, 1988, 37: 255−339.

[14] ALEXANDROV D V, DANILOV D A, GALENKO P K. Selection criterion of a stable dendrite growth in rapid solidification [J]. International Journal of Heat and Mass Transfer, 2016, 101: 789−799.

[15] KARMA A. Phase-field formulation for quantitative modeling of alloy solidification [J]. Physical Review Letters, 2001, 87: 115701.

[16] GALENKO P K, ANKUDINOV V. Local non-equilibrium effect on the growth kinetics of crystals [J]. Acta Materialia, 2019, 168: 203−209.

[17] TURNBULL D. On the relation between crystallization rate and liquid structure [J]. The Journal of Physical Chemistry, 1962, 66: 609−613.

[18] AZIZ M J, BOETTINGER W J. On the transition from short-range diffusion-limited to collision-limited growth in alloy solidification [J]. Acta Metallurgica et Materialia, 1994, 42: 527−537.

[19] DIVENUTI A G, ANDO T A. Dendrite growth model accommodating curved phase boundaries and high peclet number conditions [J]. Metallurgical and Materials Transactions A—Physical Metallurgy and Materials Science, 1998, 29: 3047−3056.

[20] SOBOLEV S L. New interpretation of experimental data on Si−As alloy solidification with planar interface [J]. Transactions of Nonferrous Metals Society of China, 2015, 25: 2797−2806.

[21] GALENKO P K, DANILOV D A. Local nonequilibrium effect on rapid dendritic growth in a binary alloy melt [J]. Physics Letters A, 1997, 235: 271−280.

[22] WANG Hai-feng, LIU Feng, CHEN Zheng, YANG Gen-chang, ZHOU Yao-he. Analysis of non-equilibrium dendrite growth in a bulk undercooled alloy melt Model and application [J]. Acta Materialia, 2007, 55: 497−506.

[23] LI Shu, ZHANG Jiong, WU Ping. Analysis for free dendritic growth model applicable to nondilute alloys [J]. Metallurgical and Materials Transactions A, 2012, 43: 3748−3754.

[24] LI Shu, ZHANG Jiong, WU Ping. A comparative study on migration of a planar interface during solidification of non-dilute alloys [J]. Journal of Crystal Growth, 2010, 312: 982−988.

[25] LI Shu, ZHANG Jiong, WU Ping. Numerical solution and comparison to experiment of solute drag models for binary alloy solidification with a planar phase interface [J]. Scripta Materialia, 2010, 62: 716−719.

[26] ECKLER K, HERLACH D M, AZIZ M J. Search for a solute-drag effect in dendritic solidification [J]. Acta Metallurgica et Materialia, 1994, 42: 975−979.

[27] WANG Hai-feng, LIU Feng, ZHAI Hai-ming, WANG Kang. Application of the maximal entropy production principle to rapid solidification: A sharp interface model [J]. Acta Materialia, 2012, 60: 1444−1454.

[28] SOBOLEV S L. Comparative study of solute trapping and gibbs free energy changes at the phase interface during alloy solidification under local nonequilibrium conditions [J]. Journal of Experimental and Theoretical Physics, 2017, 124: 459−468.

[29] GALENKO P K. Extended thermodynamical analysis of a motion of the solid-liquid interface in a rapidly solidifying alloy [J]. Physical Review B, 2002, 65: 144103.

[30] AZIZ M J, KAPLAN T. Continuous growth model for interface motion during alloy solidification [J]. Acta Metallurgica, 1988, 36: 2335−2347.

[31] KITTL J A, SANDERS P G, AZIZ M J, BRUNCO D P, THOMPSON M O. Complete experimental test of kinetic models for rapid alloy solidification [J]. Acta materialia, 2000, 48: 4797−4811.

[32] HILLERT M. Solute drag, solute trapping and diffusional dissipation of Gibbs energy [J]. Acta Materialia, 1999, 47: 4481−4505.

[33] WANG Kang, WANG Hai-feng, LIU Feng, ZHAI Hai-ming. Modeling dendrite growth in undercooled concentrated

multi-component alloys [J]. Acta Materialia, 2013, 61: 4254−4265.
[34] SOBOLEV S L. Rapid solidification under local non-equilibrium conditions [J]. Physical Review E, 1997, 55: 6845−6854.
[35] ECKLER K, COCHRANE, HERLACH D M, FEUER-BACHER B, JURISCH M. Evidence for a transition from diffusion-controlled to thermally controlled solidification in metallic alloys [J]. Physical Review B, 1992, 45: 5019−5022.
[36] ZHANG Yu-bing, DU Jing-lian, WANG Kang, WANG Hui-yuan, LI Shu, LIU Feng. Application of non-equilibrium dendrite growth model considering thermo-kinetic correlation in twin-roll casting [J]. Journal of Materials Science and Technology, 2020, 44: 209−222.
[37] PENG Hao-ran, LIU bi-shan, LIU Feng. A strategy for designing stable nanocrystalline alloys by thermo-kinetic synergy [J]. Journal of Materials Science and Technology, 2020, 43: 21−31.

考虑热力学和动力学相关性的二元合金凝固界面动力学建模

李 述[1,2]，张玉兵[1]，王 慷[1]，刘 峰[1]

1. 西北工业大学 凝固技术国家重点实验室，西安 710072；
2. 哈尔滨理工大学 理学院，哈尔滨 150080

摘 要：在同时考虑碰撞限制生长模式和短程扩散限制生长模式的情况下，提出一个更加完善且具有可变动力学前因子的二元合金固−液界面动力学模型。与上述两种生长模式相耦合，提出 4 种潜在的热力学和动力学相关性，并将其应用于平界面迁移和枝晶凝固。其中，有效热力学驱动力与有效动力学能垒间的线性相关性更符合物理实际。基于此线性热力学和动力学相关性，对于 Ni−0.7at.%B 合金，扩展的自由枝晶生长模型所得结果与实验数据吻合更好。与不变的动力学前因子模型比较可知，通常发生在合金低过冷凝固过程中的界面迁移变缓现象是热力学和动力学两种因素共同作用的结果。由热力学和动力学相关性的普适性可知，在合金凝固的界面动力学建模中应该考虑热力学和动力学的相关性。

关键词：建模；界面；枝晶凝固；二元合金；热力学；动力学；相关性

(Edited by Wei-ping CHEN)